Published in final edited form as:
J Mech Behav Biomed Mater. 2014 January ; 29: . doi:10.1016/j.jmbbm.2013.03.027.

Material Properties of the Posterior Human Sclera☆

Rafael Grytz[a], **Massimo A. Fazio**[a], **Michael J.A. Girard**[b], **Vincent Libertiaux**[a], **Luigi Bruno**[c], **Stuart Gardiner**[d], **Christopher A. Girkin**[a], and **J. Crawford Downs**[a,*]

[a]Ophthalmology, University of Alabama at Birmingham, Birmingham, Alabama, USA

[b]Bioengineering, National University of Singapore, Singapore

[c]Mechanical Engineering, University of Calabria, Cosenza, Italy

[d]Devers Eye Institute, Portland, Oregon, USA

Abstract

To characterize the material properties of posterior and peripapillary sclera from human donors, and to investigate the macro- and micro-scale strains as potential control mechanisms governing mechanical homeostasis. Posterior scleral shells from 9 human donors aged 57–90 years were subjected to IOP elevations from 5 to 45 mmHg and the resulting full-field displacements were recorded using laser speckle interferometry. Eye-specific finite element models were generated based on experimentally measured scleral shell surface geometry and thickness. Inverse numerical analyses were performed to identify material parameters for each eye by matching experimental deformation measurements to model predictions using a microstructure-based constitutive formulation that incorporates the crimp response and anisotropic architecture of scleral collagen fibrils. The material property fitting produced models that fit both the overall and local deformation responses of posterior scleral shells very well. The nonlinear stiffening of the sclera with increasing IOP was well reproduced by the uncrimping of scleral collagen fibrils, and a circumferentially-aligned ring of collagen fibrils around the scleral canal was predicted in all eyes. Macroscopic in-plane strains were significantly higher in peripapillary region then in the mid-periphery. In contrast, the meso- and micro-scale strains at the collagen network and collagen fibril level were not significantly different between regions. The elastic response of the posterior human sclera can be characterized by the anisotropic architecture and crimp response of scleral collagen fibrils. The similar collagen fibril strains in the peripapillary and mid-peripheral regions support the notion that the scleral collagen architecture including the circumpapillary ring of collagen fibrils evolved to establish optimal load bearing conditions at the collagen fibril level.

Keywords

sclera; inverse analysis; homeostasis; collagen fibril strain

☆Supported in part by U.S. Public Health Grants R01-EY18926 and R01-EY19333 from the National Eye Institute, National Institutes of Health, Bethesda, Maryland; Legacy Good Samaritan Foundation, Portland, OR; Eye Sight Foundation of Alabama; and Research to Prevent Blindness Physician-Scientist Award.

*Corresponding author: grytz@uab.edu (Rafael Grytz), cdowns@uab.edu (J. Crawford Downs).

1. Introduction

Biomechanics is likely to be important in the development and progression of glaucoma, as it provides a direct link between intraocular pressure (IOP) and the microenvironment of the optic nerve head (ONH) where glaucomatous damage to the retinal ganglion cell axons is thought to occur (Burgoyne et al., 2005; Downs et al., 2008). The sclera is an important driver of ONH biomechanics, as it imposes the principal mechanical boundary condition on the contained lamina cribrosa and neural canal tissues and the intrascleral branches of the short posterior ciliary arteries provide the primary blood supply for the lamina cribrosa. Several computational studies have shown the sclera to be among the most important determinants of ONH stress and strain (Sigal et al., 2005, 2011a,b).

Computational modeling studies are necessary to study ONH biomechanics, as no experimental methods are available to measure or estimate stress and strain in the ONH in vivo. However, without accurate material properties, these models yield inaccurate stress and strain predictions in the sclera, and hence ONH. No previous studies have reported material property estimates for the posterior and peripapillary human sclera that incorporate the inhomogeneous, hyperelastic, anisotropic nature of its material response. Histologic studies have shown that there is a circumferential ring of highly aligned collagen fibrils surrounding the ONH, and computational simulations have suggested that this ring serves to shield the relatively compliant ONH from excessive strains (Girard et al., 2009b; Grytz et al., 2011a; Coudrillier et al., 2012a). Experimental studies have shown that the sclera's mechanical response changes in response to age (Girard et al., 2009c; Coudrillier et al., 2012b) and exposure to chronically elevated IOP (Girard et al., 2011b), although no work has been done to elucidate the mechanical factors driving these changes.

In this study, we estimated eye-specific scleral material properties by matching the inflation response of an eye-specific computational model to the experimentally measured displacements of the same posterior scleral shell subjected to an inflation test. The material properties were iteratively fit to a mechanistic constitutive model formulated such that its parameters capture physiologically relevant mechanical behavior at the macro- and micro-scale. This constitutive model represents the collagen fibril, network, and non-fibrillar extracellular matrix (ECM) as separate components that combine to determine the overall mechanical response of the tissue. As such, the material properties fit with this mechanistic model can help elucidate the mechanisms underlying changes in scleral biomechanics with age, race, and IOP-driven remodeling associated with aging or disease. This is not the case with many existing phenomenological constitutive models (Coudrillier et al., 2012b; Downs et al., 2005; Elsheikh et al., 2010; Woo et al., 1972), which are accurate mathematical descriptions of the mechanical behavior but lack parameters that describe the underlying behavior of the connective tissue constituents, e.g., collagen fibrils and non-fibrillar extracellular matrix (ECM).

The sclera is a living soft tissue and its material properties evolve and change over time e.g. through growth remodeling of its collagen structure. The underlying stimuli remain unclear, although different mechanical stimuli have been proposed to drive growth and remodeling in collagenous soft tissues. Most existing computational formulations use macroscopic stress or strain variables at the tissue level to motivate growth and remodeling (Taber and Humphrey, 2001; Gleason and Humphrey, 2004; Hariton et al., 2007; Ricken et al., 2007; Driessen et al., 2004; Kuhl et al., 2005; Himpel et al., 2008; Kuhl and Holzapfel, 2007; Driessen et al., 2008; Hariton et al., 2007; Grytz and Meschke, 2010; Grytz et al., 2011a). An increasing number of studies of anisotropic growth and remodeling theories assume the existence of a homeostatic tissue strain or stress value in the direction of the collagen fibril (Watton et al., 2009; Nagel and Kelly, 2012; Zeinali-Davarani et al., 2011a, b; Martufi and Gasser, 2012).

Recently, we proposed a homeostatic strain control mechanism at the collagen fibril level to motivate the thickening of the lamina cribrosa in early stages of experimental glaucoma (Grytz et al., 2011b). Recent experimental evidence also points toward the existence of a homeostatic control mechanism at the collagen fibril level in collagenous soft tissues (Camp et al., 2011; Flynn et al., 2010; Bhole et al., 2009; Foolen et al., 2010). To investigate the potential homeostatic strain control mechanism in the posterior sclera, we calculated the relative differences in different strain variables across the scleral shell. We computed strain variables at the different length scales of our constitutive model to determine if these variables were uniform across the scleral shell and therefore could be considered as candidate variables driving homeostatic strain control.

The outline of this manuscript is as follows. In Section 2 the experimental and computational methods are presented that were used to estimate the material properties of the posterior human sclera. The results of the inverse analysis and the investigation of the different strain measures are presented in Section 3. We discuss the obtained results and the limitations of this study in Section 4. The theoretical background of our microstructure based constitutive formulation and the calculation of the cost function, which was used for the inverse analysis, are summarized in the Appendices Appendix A and Appendix B, respectively.

2. Materials and Methods

2.1. Inflation Testing and Laser Speckle Interferometry

2.1.1. Human Donor Specimens—Nine pairs of eyes from normal human donors aged 20 to 90 years old (average age of 56.7, 12 Males, 8 Females) were obtained from the Lions Eye Bank of Oregon in Portland, Oregon and the Alabama Eye Bank in Birmingham, Alabama. Donor eyes were deemed normal by next-of-kin questionnaire; donors with a history of glaucoma, severe myopia, diabetes, or gross anatomic abnormalities on inspection were excluded. All specimens were stored in isotonic saline at 4°C immediately after enucleation and tested within 48 hours post mortem as follows.

The surface strain data for these donor eyes were published in a previous report focused on regional and sectorial mechanical strain variations calculated directly from experimental inflation tests (Fazio et al., 2012). In the current study, we fit our mechanistic constitutive model formulation to the inflation test displacement data using a new inverse finite element technique in order to estimate material property parameters for these same eyes.

2.1.2. Inflation Testing, B-spline Based Displacement Fitting—The custom scleral inflation testing apparatus and general protocol used in this work has been described in previous studies (Fazio et al., 2012; Girard et al., 2009a,c). Briefly, the scleral inflation testing apparatus consists of a clamping stage with a sealed chamber atop, which allowed the posterior third of the eye to be pressurized while the spezimen was immersed in physiologic phosphate buffered saline solution (PBS). Each eye was preconditioned using 20 pressurization cycles at a rate of 5 mmHg per second and then allowed to recover for 15 minutes. Each eye was then pressurized from 5 to 45 mmHg in small steps of 0.01 to 0.2 mmHg, while scleral surface displacements were recorded using a commercial laser speckle interferometer (ESPI; Q-100, Dantec Dynamics A/S, Denmark). A starting pressure of zero could not be used since the posterior scleral shell does not maintain its shape at that pressure. The pressure testing was performed at room temperature.

Following inflation testing, the outer surface of each posterior sclera was acquired using a 3D digitizer (MicroScribe G2X, Immersion, San Jose, CA; nominal resolution of ~0.2 mm) while the shell was pressurized to 10 mmHg. A customized B-spline fitting system was used

for obtaining continuous and differentiable analytical functions that define the three-dimensional displacement field over the entire posterior third of the scleral surface as described previously (Fazio et al., 2012). Scleral thickness was measured with ultrasound at 20 predetermined locations as previously described (Girard et al., 2009a) and then continuously interpolated between the discrete measurement locations. The ONH tissues were assumed to be the same thickness as the surrounding sclera (i.e., thickness was interpolated continuously across the posterior pole). These surface geometry and scleral thickness data were combined into eye-specific finite element models as described below.

2.2. Microstructure-based constitutive model

The mechanical response of the human sclera is determined by the material properties and structural morphology of its constituents: collagen fibrils, elastin, cross-link density, non-fibrillar ECM and other constituents. As part of our ongoing efforts to elucidate the intrinsic material properties of ocular tissues, we developed a microstructure-based constitutive theory that incorporates the crimping and anisotropic orientation distribution of collagen fibrils, wherein fibrillar collagen is assumed to be the main load-bearing constituent of the load-bearing ocular tissues (Grytz, 2008; Grytz and Meschke, 2009, 2010).

2.2.1. Micro-scale—At the micro-scale, scleral collagen fibrils crimp or buckle as IOP is lowered and the fibrils become unloaded. Grytz and Meschke (2009) derived the one-dimensional elastic response of a collagen fibril assuming that the fibril crimps into a helix when unloaded (Figure 1). The collagen fibril uncrimps under tension, which leads to the nonlinear stiffening typical of collagenous tissue. The stretch level at which the collagen fibrils straighten marks a characteristic point in the nonlinear elastic (stress-strain) response of the model and is hereafter called the locking stretch. The elastic response of the collagen fibril is defined by one stiffness parameter, the elastic modulus of the collagen fibril E_{fib}, and two micro-structural parameters that define its crimp geometry, the crimp angle θ_0 and ratio between the crimp amplitude and the fibril crossectional radius R_0/r_0.

2.2.2. Meso-scale—At the scleral meso-scale, collagen fibrils aggregate and form complex architectures with directional (anisotropic) stiffness. We assume that collagen fibrils are tangent to the scleral surface as observed in previous histologic studies (Watson and Young, 2004). We use a semicircular von Mises distribution function to describe the anisotropic collagen fibril orientation distribution in which ϕ_p is an angle that defines the preferred orientation and b is the concentration parameter of the collagen fibril distribution (Figure 1) (Grytz, 2008; Girard et al., 2009b). Collagen fibrils are randomly oriented in the scleral plane for $b = 0$ and become increasingly aligned along the preferred orientation for increasing values of b. A detailed discussion on the anisotropic material response for varying meso-structural parameters is provided in our previous publication (Girard et al., 2009b).

2.2.3. Macro-scale—We assume that the anisotropic collagen network is embedded in a nearly incompressible non-fibrillar tissue matrix with isotropic (orientation independent) material properties. This isotropic tissue matrix represents all non-collagenous tissue components (e.g., elastin, glycosaminoglycans, proteoglycans, cells, and fluid), as well as the isotropic component of the collagen fibril network. The isotropic elastic response of the tissue matrix is described by the shear modulus μ.

In total, the constitutive model contains two micro-structural parameters (θ_0, R_0/r_0), two meso-structural parameters (ϕ_p, b), and two stiffness parameters (μ, E_{fib}). In contrast to phenomenological constitutive models that describe elastic behavior but whose formulation has no physical relevance (Coudrillier et al., 2012b; Downs et al., 2005; Elsheikh et al.,

2010; Woo et al., 1972), the structural parameters of our mechanistic model have clear physical interpretations and can be directly obtained from experimental observations. The strain energy density function and main equations of the constitutive theory are presented in Appendix Appendix A.

2.3. Eye-specific finite element (FE) modeling

2.3.1. FE mesh—The surface geometry and thickness of each posterior scleral shell was obtained experimentally as described above and combined to generate eye-specific FE models. The FE mesh was comprised of 256 quadratic hexahedral elements for the posterior sclera and 80 for the ONH using one element through the shell thickness (Figure 2a). We used a fitted, eye-specific model to test the appropriateness of this mesh density in terms of numerical accuracy. This mesh convergence test showed that doubling the mesh density in both in-plane directions and in thickness direction changed the displacement predictions of the model by less than 5%. Based on this test the mesh density was considered sufficient to ensure numerical accuracy of the results.

2.3.2. Boundary conditions—The posterior sclera for each eye was clamped to a custom-built pressurization apparatus to determine inflation-induced displacements. Scleral clamping was achieved by positioning the posterior scleral shell onto a radiused plastic ring and then elevating a vertical stage to squeeze the sclera between the ring and the machined conical surface of a fixed, stainless steel clamping plate. Modeling the mechanical boundary conditions at the scleral clamping site presents several challenges, as the clamping process squeezes and prestresses the tissue and the degree to which the clamping process constraints the deformation of the scleral shell is likely eye-specific. Previously, we assumed that scleral deformations were perfectly constrained throughout the scleral thickness between the plastic ring and the clamping plate (a fixed boundary condition) (Girard et al., 2009a). Preliminary studies showed that this approach is reasonable for nonhuman primate scleral shells but over constrains human scleral shells, which is likely due to the significantly greater thickness of human sclera. As a result, we used eye-specific boundary conditions that allow us to adjust the stiffness of the clamping constraint such that the computational model best fit the experimental displacements. At the clamp, we assume a simple support at the outer surface of the sclera and spring support through the scleral thickness (Figure 2b). Our experimental clamping condition does not result in a perfectly rigid support, and therefore this spring support represents the experimental condition more accurately than a fixed boundary condition. The eye-specific boundary conditions require the fit-ting of a spring stiffness k for each eye, which was fitted as an unknown parameter in the inverse identification algorithm presented in the subsequent section. The fitted eye-specific boundary conditions were found to significantly improve the quality of the material property fits compared to a fixed boundary condition.

2.3.3. Extended FE mesh—To model local differences in tissue anisotropy (Zeinali-Davarani et al., 2011a), we used an extended mesh on the outer scleral surface that allowed us to interpolate the meso-structural parameters (phi_p, b) across the entire posterior scleral shell beyond the clamp boundary (Figure 2c). The extended mesh contains 16 control points at which the parameters phi_p, b must be defined. The extended mesh is defined with respect to a spherical coordinate system, which was defined such that the polar axis is going through the center of the ONH and the origin of a sphere that best fits the posterior scleral shell (see Figure 1). A standard bi-linear interpolation along the spherical coordinates is performed for each element of the extended mesh. The interpolated values are used to solve the constitutive equations at each Gauss point of the regular (non-extended) FE mesh (Appendix Appendix A).

2.4. Inverse parameter identification

2.4.1. Model assumptions—We assume that the stiffness parameters (μ, E_{fib}), as well as the micro-structural parameters (θ_0, R_0/r_0) are uniform across the entire scleral shell for each eye. The meso-structural parameters that define local anisotropy (ϕ_p, b) are defined at the 16 control points of the extended mesh. To reduce the number of unknowns, further assumptions were made regarding the meso-structure. In accordance with previous experimental (Goldbaum et al., 1989; Winkler et al., 2010) and numerical studies (Grytz et al., 2011a), the alignment of collagen fibrils around the scleral canal was assumed to be circumferential by setting $\phi_p = 0$ and $b = 10$ at control points 1–4 (Figure 2). At the equator, collagen fibrils were assumed to be planar isotropic by setting $\phi_p = 0$ and $b = 0$ at control points 13–16. To further reduce the number of unknowns, the preferred orientation angles at the periphery of the scleral shell ($\phi_{p,9} = \phi_{p,10} = \phi_{p,11} = \phi_{p,12}$) were assumed to be identical. In total, the inverse FE problem for each eye consisted of 21 unknown parameters as summarized in Table 1. The lower and upper limits assumed for each parameter (Table 1) were enforced by using the bounce back method (Price et al., 2005).

For the sake of simplicity, the ONH tissues (including the lamina cribrosa) were modeled by interpolating the scleral thickness measurements across the scleral canal. To compensate for the ONHs lower structural stiffness, which results from the significantly lower thickness and collagen fibril density of the lamina cribrosa compared with the surrounding sclera, the stiffness parameters of the ONH were reduced by a factor of 15 compared to the scleral values ($E_{\text{fib,ONH}} = E_{\text{fib,Sclera}}/15$). The micro-structural parameters (θ_0, R_0/r_0) were set to the scleral values. The ONH was also assumed to have planar isotropic oriented collagen fibrils ($b_{\text{ONH}} = 0$).

2.4.2. Cost function—A crucial part of any inverse optimization scheme is the definition of an objective cost function that defines the quality of the fit. Let cost be the cost function that must be minimized by the optimization algorithm. We propose a cost function that is based on the sum of squared residuals (error) when comparing the FE model and experimental displacements, integrated over the outer surface of the sclera. To accurately capture the nonlinear stiffening of the sclera, we sum the cost over nine IOP elevation ranges (from 5 mmHg to 7, 10, 15, 20, 25, 30, 35, 40, and 45 mmHg). The cost function is both normalized and weighted such that each IOP level and each displacement component (X, Y, and Z) has a similar overall impact on the cost function. Detailed derivations of the cost function are presented in Appendix Appendix B. To neglect unphysical solutions from the search space of the fitting algorithm, a penalty function, *penalty*, was used. The penalty function was defined based on the assumption that at least 80% of scleral collagen fibrils uncrimp for a pressure elevation from 5 to 45 mmHg (see Appendix Appendix B). The penalty function was found to effectively remove unphysical solutions and to improve the convergence rate of the inverse problem.

2.4.3. Global optimization approach—The inverse finite element problem of each posterior scleral shell presents a large-scale optimization problem characterized by multiple local minima in the cost function. The differential evolution (DE) approach initially proposed by Storn and Price (1997) has proven to be a robust algorithm in many applications that converges faster and with more certainty than many other global optimization schemes. Recent advances in the DE approach were summarized by Neri and Tirronen (2010). We use the DE algorithm recently proposed by Brest and Maučec (2010). This algorithm was designed to solve large-scale optimization problems with multiple local minima similar to the inverse problem presented here. The initial control parameters of the algorithm were chosen as proposed by Brest and Maučec (2010) except for the maximum

number of iterations, which was set to 2000. We tested the convergence properties and the repeatability of the method by solving five independent trials for two inverse problems.

2.4.4. High Performance Computing (HPC)—Global optimization schemes such as the algorithm used in this study require a large number of cost function computations (number of iteration times the size of the population). In the present case, each cost calculation represents the solution of a nonlinear eye-specific FE model, which takes about 1 to 1.5 minutes solution time on a standard PC. Approximately 47,000 cost calculations are necessary to perform one eye-specific scleral material property fit, which would require 33–51 days on a standard PC. To handle this high demand on computational calculations in a reasonable amount of time, a parallelized solution strategy was developed. DE algorithms are parallel in nature and well suited for parallel computing strategies. We developed a HPC strategy that largely follows a master-slave scheme running on approximately 160 idle CPU cores distributed among the Apple Mac Pro workstations in our department. This HPC setup led to an average solution time of 13 hours for each eye-specific global optimization problem.

2.4.5. Pre-stress—In general, the posterior human sclera maintains its spherical shape at zero IOP but it may buckle locally. To exclude the potential for unbuckling of the scleral shell during the inflation tests, we preloaded the shells with 5 mmHg IOP prior to displacement recording (Fazio et al., 2012). This preload induces a prestress state that needs to be taken into account in the inverse parameter identification process if one seeks to identify the intrinsic material properties of the sclera. The FE-mesh was constructed using scleral surface geometric information collected at an IOP of 10 mmHg (Fazio et al., 2012) while the preload of the tissues for the inflation test was 5 mmHg. The scleral shell deforms from 0 to 10 mmHg, but these deformations are small (Fazio et al., 2012), and below the 250 μm resolution of the 3D digitizer we used to collect the scleral surface geometry data. We recently proposed a new numerical method (Grytz and Downs, 2012) to accurately calculate this pre-existing stress state. However, we have also shown that an indirect approach (Grytz and Meschke, 2010; Grytz and Downs, 2012) using relative displacements was suitable for the inverse parameter identification of scleral elasticity from inflation tests. The indirect approach requires significantly less computational time than the accurate method and was found to perform better (Grytz and Downs, 2012) compared to an alternative approach based on relative IOP values (Girard et al., 2009a,c). Considering the large number of calculations and the associated computational cost, we applied the indirect method using relative displacements (Grytz and Downs, 2012) in the present study to estimate the pre-stressed state of each eye.

2.5. Strain Variables as Candidates for Homeostatic Control

To determine if tissue and fibril level strains were uniform across the posterior sclera and therefore could be considered as candidate variables for homeostatic strain control, we investigated the relative differences in strain across the scleral shell at the macro-scale and collagen fibril level. To accomplish this, the results of the inverse FE models were analyzed with respect to strain predictions obtained at the different length scales of the multi-scale model. We used four strain-based measures: (i) the *in-plane strain*, which represents the average tissue strain in the scleral shell plane; (ii) the *collagen network strain*, which represents the average axial strain within the dispersed collagen fibril orientations; (iii) the *collagen fibril strain*; and (iv) the percentile of *locked collagen fibrils*, which represents the percentile of scleral collagen fibrils that are straightened (un-crimped). The mathematical definition of the different strain-based values can be found in Appendix Appendix A and a graphical illustration of the *collagen fibril strain* is shown in Figure 1. Average strain-based measures were computed for the peripapillary and mid-peripheral regions. The peripapillary

region was defined as a 10-degree-wide band adjacent to the ONH (approximately 2.2 mm wide) and the mid-peripheral region was defined for each eye such that it had the same surface area as the peripapillary region. We calculated the volume average of the strain responses in these two regions within each eye. We used linear mixed effects statistical models, which account for the difference between intra- and inter-donor variability, to determine if strains were significantly different between the two regions.

The overall IOP-dependent elastic response of the inverse model is primarily dictated by the two stiffness parameters (μ, E_{fib}) and the two micro-structural parameters (θ_0, R_0/r_0). To investigate the variation and the biomechanical implications of these model parameters on IOP-dependent scleral elasticity, a parametric study was performed. The eye-specific model that exhibited the set of fitted model parameters closest to the mean values for the entire group was used for the parametric study. To investigate the sensitivity and physical interpretations of the material property parameters, the four strain-based measures introduced above were computed for the peripapillary and mid-peripheral region by setting one of the four constitutive parameters to the minimum and maximum values of the fitted range while keeping the other parameters at their mean values.

3. Results

3.1. Convergence and Repeatability

To test the convergence properties and the repeatability of the global optimization approach, five independent trials of the inverse problem for both eyes of Donor 1 were solved with inputs randomly chosen from within the minimum and maximum limits stated in Table 1. The fitted material and micro-structural parameters for the different trials are presented in Table 2. The five trials of both eyes yield nearly identical results, with less than 0.5% difference between the fitted model parameters. These results suggest that the self-adaptive global DE optimization approach can effectively reproduce a global convergence of the inverse problems within 2,000 iterations.

3.2. Inverse FE Results

The fitted stiffness and micro-structural parameters of each eye are presented together with their minimized cost values in Table 3. The results show a wide variability for the shear modulus, elastic modulus, and collagen fibril geometry ratio R_0/r_0. Figure 3 shows that the three-dimensional experimental displacements are a close match to the numerical predictions for both eyes of Donor 1, which was typical for all eyes in the study. The predicted FE displacements were in good agreement with both: (i) the overall nonlinear displacement response at the different IOP levels between 5 and 45 mmHg, and (ii) the localized deformation patterns of the experimental measurements. The fitted predominant collagen orientation maps for these two eyes are also shown in Figure 3, showing the circumpapillary ring of collagen fibrils. Figure 4 shows the average predominant collagen fibril orientations averaged across all eyes, plotted for eight sectors of the peripapillary and mid-peripheral regions, respectively. All eyes were characterized by a circumferentially aligned ring of collagen fibrils in the peripapillary region and a more random fibril distribution in the peripheral sclera. It should be noted that a circumpapillary ring of collagen fibrils was the initial condition in the models, but its dimension and the degree to which the fibrils orient away from the circumferential direction was fit along with the remainder of the parameters.

The predicted *in-plane strain*, the *collagen network strain*, the *collagen fibril strain*, and the percentile of *locked collagen fibrils*, are plotted for each eye together with the mean response in Figure 5. A large variability can be observed throughout the four strain-based responses. While the in-plane strain is significantly higher in the peripapillary region ($p <$

0.001), there are no significant regional differences in the collagen network and fibril strains (p = 0.11 and 0.34, respectively). For IOP ranges between 0 to ~20 mmHg, the in-plane and the collagen network strain curves show a nonlinear stiffening of the tissue and the collagen network, respectively. These strain responses become almost linear for IOPs larger than 20 mmHg, because the majority of collagen fibrils have straightened (locked) at that IOP. At the collagen fibril level, the strains follow an almost linear pattern through the entire IOP range. The collagen fibril strains at the micro-scale are much smaller than the strain measures at the higher scales. At an IOP of 15 mmHg, the mean values of the collagen fibril strain over both regions was 0.046 ± 0.025%, collagen network strain was 0.44±0.2%, and the in-plane strain was 1.09 ± 0.48%. In both regions, the percentile of fibrils that are stretched beyond their locking point increases with IOP, and the majority of collagen fibrils are recruited to participate in bearing the IOP load between 7 and 20 mmHg.

3.3. Parameter study

The right posterior scleral shell of donor 7 was used for a parametric study as its fitted model parameters were closest to the mean values of all the eyes in this study. The independent effects of the two macro-structural (μ, E_{fib}) and two micro-structural parameters (θ_0, R_0/r_0) on the *in-plane strain*, the *collagen network strain*, the *collagen fibril strain*, and the percentile of *locked collagen fibrils* are shown in Figure 6. For each parameter, the response curves for the maximum, minimum, and mean parameter values (Table 3) were compared, while the other model parameters were kept at their mean values.

At the macro-scale, the *in-plane strain* was higher in the peri-papillary region compared to the mid-periphery for each of the parameter variations. An increasing shear modulus (μ) led to an overall stiffening of the tissue and vice-versa. An increase in the elastic modulus of collagen fibrils (E_{fib}) increased the tissue stiffness at IOP levels 10 mmHg and higher and vice-versa. An increasing collagen fibril crimp angle (θ_0) increases the *in-plane strain* by a constant shift of the response curve and vice-versa. Variation in the collagen fibril geometry ratio R_0/r_0 only had a very small impact on the tissue stiffness around the transition region between the soft and stiff tissue response (at an IOP of ~10 mmHg).

At the meso-scale, the aforementioned parameter variations elicited similar effects on the *collagen network strain* curves compared to the *in-plane strain* except for the following observations: the IOP-dependent *collagen network strains* are almost identical for the peripapillary and mid-peripheral regions; the shear modulus has an significant lower impact on the *collagen network strain* compared to the *in-plane strain*; and variations in the collagen crimp angle have the greatest impact on the variation of *collagen network strain*.

At the micro-scale, the *collagen fibril strain* and the percentile of *locked collagen fibrils* were similar between the peri-papillary and mid-peripheral regions for the different parameter variations. The elastic modulus of the collagen fibrils had the most significant effect on the *collagen fibril strains*.

4. Discussion

An inverse numerical fitting strategy was proposed to identify material properties of posterior human scleral shells using three-dimensional, full-field displacement measurements from experimental inflation tests. The model is based on a mechanistic constitutive formulation (Grytz and Meschke, 2009) that derives the inhomogeneous, hyperelastic, and anisotropic nature of the scleral material response from the microstructure collagen fibrils. The proposed inverse model was found to reproduce both the overall and local deformation response of the posterior scleral shells from individual eyes. The fitted material parameters of our mechanistic model have a clear physical meaning and can be

compared to direct experimental observations. As such, the material properties fit with this model can help elucidate the mechanisms underlying micro- and macroscopic changes in scleral biomechanics with age, race, and IOP-driven remodeling in glaucoma.

The proposed constitutive model is based on the sum of isotropic and anisotropic strain energies, where the latter is assumed to represent the elastic contribution of the anisotropic collagen fibril architecture. Based on the 9 pairs of human eyes investigated here (57–90 years old), the inverse analysis showed a large variation in the estimated model parameters. The estimated elastic modulus (per tissue volume) of collagen fibrils, E_{fib}, was 41.83 ± 23.37 MPa (mean, standard deviation) and the crimp angle of collagen fibrils, θ_0, was 5.35 ± 1.28 degrees. These values are very close to our previous estimates (E_{fib} = 37.42 MPa, θ_0 = 5.09 deg) (Grytz, 2008; Grytz and Meschke, 2010), which were based on fitting parameters to experimental inflation measurements for a single meridional section as reported by Woo et al. (1972). The estimated shear modulus of the human sclera (μ = 0.33 ± 0.2 MPa) and the ratio between the crimp amplitude and cross section radius of collagen fibrils (R_0/r_0 = 4.54 ± 2.6) were significantly higher than our previous estimates of 0.01 MPa and 1.09, respectively (Grytz, 2008; Grytz and Meschke, 2010). This difference may be the result of the much simpler modeling approach used in our previous work (Grytz, 2008; Grytz and Meschke, 2010) and/or the one-dimensional displacement measurements by Woo et al. (1972). The three-dimensional, full-field displacement measurements, coupled with the much more sophisticated modeling and fitting approach used here, provide the best estimates reported to date for human scleral material properties. The rather high shear stiffness we report may relate to a high concentration of collagen crosslinks or the existence of a large isotropic component of the collagen fibril network, the presence of which has been suggested by Girard et al. (2011a) based on recent work in the rat sclera.

We also estimated local differences in the anisotropic collagen fibril architecture for each eye. While the model parameters associated with scleral collagen fibril anisotropy were constrained within certain limits, recurring structures were observed in the fitted results. A circumpapillary ring of collagen fibrils surrounding the scleral canal was a characteristic structure in all eyes, which is in agreement with experimental observations (Goldbaum et al., 1989; Winkler et al., 2010; Girard et al., 2011a; Pijanka et al., 2012) and previous numerical predictions (Girard et al., 2009a; Grytz et al., 2011a; Girard et al., 2011b). At the periphery of the posterior sclera, collagen fibrils were estimated to be more randomly oriented, which has also been observed experimentally (Boote et al., 2010).

The use of a microstructurally motivated constitutive model allowed for the numerical investigation of IOP-dependent scleral strains at different length scales that have different interpretations and ramifications. At the macro-scale, the in-plane strains were found to be significantly higher in peripapillary region than in the mid-periphery, which matches our recent direct calculations of macro-scale scleral strain in these same eyes (Fazio et al., 2012). In contrast, the collagen network and collagen fibril strains that occur at the meso- and micro-scale were very similar in both regions. This finding has implications for both the resident cell populations and in determining the biomechanical signals and mechanisms that drive IOP-related scleral remodeling processes. These findings suggest that the fibril-level strains are a candidate for driving the mechanisms that maintain scleral mechanical homeostasis, while the tissue level strains are not good candidates.

We have previously shown that the sclera stiffens in the monkey eye when exposed to chronic IOP elevations (Girard et al., 2011b). We hypothesized that this stiffening is a remodeling mechanism that strives to maintain homeostatic loading conditions at the collagen fibril level (Grytz et al., 2012). Recent experimental evidence supports the hypothesis that evolution, growth and remodeling mechanisms in soft collagenous tissues

are driven by the loading conditions of the collagen fibrils themselves (Camp et al., 2011; Flynn et al., 2010; Foolen et al., 2010). Our finding that the *collagen network strain* and *collagen fibril strain* are similar in the peripapillary and mid-peripheral regions even though the macro-scale *in-plane strains* are different support this hypothesis. This finding also supports that both strain measures, the *collagen network strain* and *collagen fibril strain*, are reasonable candidate variables to drive homeostatic strain control in the sclera. In addition, previous modeling studies have shown that IOP-related stress concentrates around the scleral canal due to the presence of the more compliant ONH. Our results further suggest that the ring of collagen fibrils around the scleral canal is necessary to establish optimal load bearing conditions at the collagen fibril level, while also protecting the contained ONH from excessive strain induced by scleral canal expansion. Previously, we estimated a homeostatic collagen fibril strain of 0.1% in our study on the remodeling of the lamina cribrosa in early glaucoma (Grytz et al., 2011b). In the present study, an average collagen fibril strain of 0.046 ± 0.025% was identified for the peripapillary and mid-peripheral region at 15 mmHg IOP. Both estimates are in the same order of magnitude, which supports the notion that collagen fibril strain of this magnitude represents a homeostatic zone for scleral collagen fibrils.

Grytz and Meschke (2009) showed that the crimp angle parameter and the collagen fibril strain predictions of the crimped collagen fibril model compare well to experimental measurements in rat tail tendons (Diamant et al., 1972) and bovine Achilles tendons (Sasaki and Odajima, 1996), respectively. The collagen architecture of the sclera appears more complex in that it incorporates interwoven and more randomly oriented lamellae. Consequently, inter-lamellar interactions are more likely to play an important role in the elastic response of the scleral collagen network. Neither fibril nor lamellar interaction have been considered in the constitutive model used here. Accordingly, it remains unclear to what extent the collagen fibril strain and the crimp angle computed in this study compare to the scleral microstructure and its deformation in the living tissue, and they should therefore only be considered as estimates.

Our constitutive formulation does not directly model the elastic response of cells, proteoglycans, elastin, glycosaminoglycans and other extracellular tissue constituents because the overall elastic response of all these constituents is combined into one parameter, the shear modulus. Consequently, the contribution of each constituent to the material properties or the interaction of these constituents with the collagen fibril network cannot be directly obtained from our results. While it would be ideal to describe these separate constituents with separate parameters in our constitutive formulation, it would also increase the number of unknown parameters that must be estimated. As our current model already incorporates an accurate mathematical description of the hyperplastic and anisotropic material response of the sclera, the elastic contribution of any additional constituent would overlap with the elastic contribution of existing parameters and diminish the repeatability and uniqueness of the inverse fitting procedure. If elastin contributes significantly to the anisotropic material response of the sclera, that behavior will be captured in the model as part of the collagen network. To incorporate additional constituents and mechanisms into our model and to further elucidate the intrinsic material properties of ocular tissues, additional experimental data will be required to eliminate additional unknowns. In this context, mechanistic constitutive models have a clear advantage over phenomenological models, as structural parameters such as the crimp angle of collagen fibrils (Diamant et al., 1972; Hill et al., 2012) and the distribution of collagen fibril orientations (Girard et al., 2011a; Pijanka et al., 2012; Meek and Quantock, 2001) can be directly obtained from experimental observations.

In other constitutive formulations, the nonlinear stiffening of soft collagenous tissues is derived from a load dependent recruitment of collagen fibrils based on a distribution of collagen fibril undulation (Cacho et al., 2007; Lokshin and Lanir, 2009; Martufi and Gasser, 2011; Raz and Lanir, 2009). We did not consider this, but assumed a constant collagen fibril crimp angle throughout the scleral shell. However, the model still predicted a nonlinear recruitment of collagen fibrils, as demonstrated by the increase in the percentile of locked fibrils with increasing IOP. This effect is mainly driven by the mechanism that in-plane strains are in general higher at the exterior than at the interior surface of scleral shells subjected to IOP. This in turn leads to an earlier recruitment of collagen fibrils at the exterior surface of the scleral model, which is a consequence of our model assumptions and might be different in the living tissue. If the homeostatic theory presented above holds and collagen fibrils are remodeled to reside at homeostatic strain in the living tissue, collagen fibrils should have a wavier structure (higher crimp angle) at the exterior surface compared to the interior surface when the sclera is unloaded. However, this mechanism remains to be experimentally investigated.

The presented inverse material property identification method presents a novel strategy to elucidate intrinsic elastic properties of the posterior sclera. The method presents a promising tool to investigate biomechanical mechanisms that may alter the elastic properties during aging or glaucoma. The parameter study quantified the effects of each of the constitutive model parameters on the overall mechanical response of the sclera, and thereby elucidates the physiological relevance of each parameter. The reported material property parameter estimates provide the most comprehensive characterization of the human scleral mechanical response, and can serve as inputs to future computational models of the posterior scleral shell and ONH.

References

Başar, Y.; Weichert, D. Nonlinear Continuum Mechanics of Solids. Springer Verlag; Berlin: 2000.

Bhole AP, Flynn BP, Liles M, Saeidi N, Dimarzio CA, Ruberti JW. Mechanical strain enhances survivability of collagen micronet-works in the presence of collagenase: implications for load-bearing matrix growth and stability. Phil Trans R Soc A. Sep; 2009 367 (1902):3339–3362. [PubMed: 19657003]

Boote C, Sorensen T, Coudrillier B, Myers K, Meek K, Quigley H, Nguyen T. Posterior scleral collagen architecture in normal and glaucoma human eyes, as determined using wide-angle x-ray scattering. ARVO Abstract. 2010; 51:4900.

Brest J, Maučec M. Self-adaptive differential evolution algorithm using population size reduction and three strategies. Soft Computing-A Fusion of Foundations, Methodologies and Applications. 2010; 15 (11):2157–2174.

Burgoyne CF, Downs JC, Bellezza AJ, Suh JKF, Hart RT. The optic nerve head as a biomechanical structure: a new paradigm for understanding the role of IOP-related stress and strain in the pathophysiology of glaucomatous optic nerve head damage. Prog Retina Eye Res. Jan; 2005 24 (1): 39–73.

Cacho F, Elbischger PJ, Rodríguez JF, Dolbaré M, Holzapfel GA. A constitutive model for fibrous tissues considering collagen fiber crimp. International Journal of Non-Linear Mechanics. 2007; 42:391–402.

Camp RJ, Liles M, Beale J, Saeidi N, Flynn BP, Moore E, Murthy SK, Ruberti JW. Molecular mechanochemistry: low force switch slows enzymatic cleavage of human type I collagen monomer. J Am Chem Soc. Mar; 2011 133 (11):4073–4078. [PubMed: 21348512]

Coudrillier B, Boote C, Quigley HA, Nguyen TD. Scleral anisotropy and its effects on the mechanical response of the optic nerve head. Biomech Model Mechanobiol. Nov.2012a (in press).

Coudrillier B, Tian J, Alexander S, Myers KM, Quigley HA, Nguyen TD. Biomechanics of the human posterior sclera: age- and glaucoma-related changes measured using inflation testing. Invest Ophthalmol Vis Sci. 2012b; 53 (4):1714–1728. [PubMed: 22395883]

Diamant J, Keller A, Baer E, Litt M, Arridge R. Collagen: Ultrastructure and its relation to mechanical properties as a function of aging. Proceedings of Royal Society of London, Series B. 1972; 180:293–315.

Downs JC, Roberts MD, Burgoyne CF. Mechanical environment of the optic nerve head in glaucoma. Optom Vis Sci. Jun; 2008 85 (6):425–435. [PubMed: 18521012]

Downs JC, Suh JK, Thomas KA, Bellezza AJ, Hart RT, Burgoyne CF. Viscoelastic material properties of the peripapillary sclera in normal and early-glaucoma monkey eyes. Invest Ophthalmol Vis Sci. 2005; 46:540–546. [PubMed: 15671280]

Driessen NJB, Cox MAJ, Bouten CVC, Baaijens PTB. Remodelling of the angular collagen fiber distribution in cardiovascular tissues. Biomech Model Mechanobio. 2008; 7:93–103.

Driessen NJB, Wilson W, Bouten CVC, Baaijens FPT. A computational model for collagen fibre remodelling in the arterial wall. J Theor Biol. 2004; 226:53–64. [PubMed: 14637054]

Elsheikh A, Geraghty B, Alhasso D, Knappett J, Campanelli M, Rama P. Regional variation in the biomechanical properties of the human sclera. Exp Eye Res. May; 2010 90 (5):624–633. [PubMed: 20219460]

Fazio MA, Grytz R, Bruno L, Girard MJA, Gardiner S, Girkin CA, Downs JC. Regional variations in mechanical strain in the posterior human sclera. Invest Ophthalmol Vis Sci. Sep; 2012 53 (9): 5326–5333. [PubMed: 22700704]

Flynn BP, Bhole AP, Saeidi N, Liles M, Dimarzio CA, Ruberti JW. Mechanical strain stabilizes reconstituted collagen fibrils against enzymatic degradation by mammalian collagenase matrix metalloproteinase 8 (MMP-8). PLoS ONE. 2010; 5 (8):e12337. [PubMed: 20808784]

Foolen J, van Donkelaar CC, Soekhradj-Soechit S, Ito K. European Society of Biomechanics S.M. Perren Award 2010: an adaptation mechanism for fibrous tissue to sustained shortening. J Biomech. Sep; 2010 43 (16):3168–3176. [PubMed: 20817184]

Girard MJA, Dahlmann-Noor A, Rayapureddi S, Bechara JA, Bertin BME, Jones H, Albon J, Khaw PT, Ethier CR. Quantitative mapping of scleral fiber orientation in normal rat eyes. Invest Ophthalmol Vis Sci. 2011a; 52 (13):9684–9693. [PubMed: 22076988]

Girard MJA, Downs JC, Bottlang M, Burgoyne CF, Suh JF. Peripapillary and posterior scleral mechanics–Part II: Experimental and inverse finite element characterization. J Biomech Eng. 2009a; 131 (5):051012. [PubMed: 19388782]

Girard MJA, Downs JC, Burgoyne CF, Suh JF. Peripapillary and posterior scleral mechanics–Part I: Development of an anisotropic hyperelastic constitutive model. J Biomech Eng. 2009b; 131 (5): 051011. [PubMed: 19388781]

Girard MJA, Suh JKF, Bottlang M, Burgoyne CF, Downs JC. Scleral biomechanics in the aging monkey eye. Invest Ophthalmol Vis Sci. Nov; 2009c 50 (11):5226–5237. [PubMed: 19494203]

Girard MJA, Suh JKF, Bottlang M, Burgoyne CF, Downs JC. Biomechanical changes in the sclera of monkey eyes exposed to chronic IOP elevations. Invest Ophthalmol Vis Sci. Aug; 2011b 52 (8): 5656–5669. [PubMed: 21519033]

Gleason RL, Humphrey JD. A mixture model of arterial growth and remodeling in hypertension: altered muscle tone and tissue turnover. J Vasc Res. 2004; 41 (4):352–363. [PubMed: 15353893]

Goldbaum MH, Jeng SY, Logemann R, Weinreb RN. The extracellular matrix of the human optic nerve. Arch Ophthalmol. Aug; 1989 107 (8):1225–1231. [PubMed: 2757554]

Grytz, R. PhD thesis. Ruhr-University Bochum; Germany: 2008. Computational modeling and remodeling of human eye tissues as biomechanical structures at multiple scales.

Grytz R, Downs JC. A forward incremental prestressing method with application to inverse parameter estimations and eye-specific simulations of posterior scleral shells. Comput Meth Biomech Biomed Eng. Jan.2012 (in press).

Grytz R, Girkin C, Libertiaux V, Downs J. Perspectives on biomechanical growth and remodeling mechanisms in glaucoma. Mechanics Research Communications. 2012; 42:92–106. [PubMed: 23109748]

Grytz R, Meschke G. Constitutive modeling of crimped collagen fibrils in soft tissues. J Mech Behavior Biomed Mat. Oct; 2009 2 (5):522–533.

Grytz R, Meschke G. A computational remodeling approach to predict the physiological architecture of the collagen fibril network in corneoscleral shells. Biomech Model Mechanobiol. Apr; 2010 9 (2):225–235. [PubMed: 19802726]

Grytz R, Meschke G, Jonas JB. The collagen fibril architecture in the lamina cribrosa and peripapillary sclera predicted by a computational remodeling approach. Biomech Model Mechanobiol. 2011a; 10 (3):371–382. [PubMed: 20628781]

Grytz R, Sigal IA, Ruberti JW, Meschke G, Downs JC. Lamina cribrosa thickening in early glaucoma predicted by a microstructure motivated growth and remodeling approach. Mech Mat. 2011b; 44:99–109.

Hariton I, de Botton G, Gasser TC, Holzapfel GA. Stress-driven collagen fiber remodeling in arterial walls. Biomech Model Mechanobiol. Apr; 2007 6 (3):163–175. [PubMed: 16912884]

Hill MR, Duan X, Gibson GA, Watkins S, Robertson AM. A theoretical and non-destructive experimental approach for direct inclusion of measured collagen orientation and recruitment into mechanical models of the artery wall. J Biomech. Feb.2012 45:762–771. [PubMed: 22305290]

Himpel G, Menzel A, AK, Steinmann P. Time-dependent fiber reorientation of transversely isotropic continua–finite element formulation and consistent linearization. Int J Numer Meth Engng. 2008; 73:1413–1433.

Kuhl E, Garikipati K, Arruda E, Grosh K. Remodeling of biological tissues: Mechanically induced reorientation of a transversely isotropic chain network. J Mech Phys Solids. 2005; 53:1552–1573.

Kuhl E, Holzapfel G. A continuum model for remodeling in living structures. J Mat Sc. 2007; 42:8811–8823.

Lokshin O, Lanir Y. Micro and macro rheology of planar tissues. Biomaterials. Jun; 2009 30 (17): 3118–3127. [PubMed: 19324407]

Martufi G, Gasser TC. A constitutive model for vascular tissue that integrates fibril, fiber and continuum levels with application to the isotropic and passive properties of the infrarenal aorta. J Biomech. Sep; 2011 44 (14):2544–2550. [PubMed: 21862020]

Martufi G, Gasser TC. Turnover of fibrillar collagen in soft biological tissue with application to the expansion of abdominal aortic aneurysms. J R Soc Interface. Aug.2012 9:3366–3377. [PubMed: 22896562]

Meek KM, Quantock AJ. The use of x-ray scattering techniques to determine corneal ultrastructure. Prog Retin Eye Res. Jan; 2001 20 (1):95–137. [PubMed: 11070369]

Nagel T, Kelly DJ. Remodelling of collagen fibre transition stretch and angular distribution in soft biological tissues and cell-seeded hydrogels. Biomech Model Mechanobiol. May.2012 11:325–339. (in press). [PubMed: 21611762]

Neri F, Tirronen V. Recent advances in differential evolution: a survey and experimental analysis. Artificial Intelligence Review. 2010; 33 (1):61–106.

Pijanka JK, Coudrillier B, Ziegler K, Sorensen T, Meek KM, Nguyen TD, Quigley HA, Boote C. Quantitative mapping of collagen fiber orientation in non-glaucoma and glaucoma posterior human scleras. Invest Ophthalmol Vis Sci. Jul; 2012 53 (9):5258–5270. [PubMed: 22786908]

Price, K.; Storn, R.; Lampinen, J. Differential evolution: a practical approach to global optimization. Springer-Verlag New York Inc; 2005.

Raz E, Lanir Y. Recruitment viscoelasticity of the tendon. J Biomech Eng. Nov.2009 131 (11):111008. [PubMed: 20353259]

Ricken T, Schwarza A, Bluhm J. A triphasic model of transversely isotropic biological tissue with applications to stress and biologically induced growth. Comput Mat Sc. 2007; 39:124–136.

Sasaki N, Odajima S. Elongation mechanism of collagen fibrils and force-strain relations of tendon at each level of structural hierarchy. J Biomech. 1996; 29:1131–1136. [PubMed: 8872269]

Sigal IA, Flanagan JG, Ethier CR. Factors influencing optic nerve head biomechanics. Invest Ophthalmol Vis Sci. Nov; 2005 46 (11):4189–4199. [PubMed: 16249498]

Sigal IA, Yang H, Roberts MD, Burgoyne CF, Downs JC. IOP-induced lamina cribrosa displacement and scleral canal expansion: an analysis of factor interactions using parameterized eye-specific models. Invest Ophthalmol Vis Sci. Mar; 2011a 52 (3):1896–1907. [PubMed: 20881292]

Sigal IA, Yang H, Roberts MD, Grimm JL, Burgoyne CF, Demirel S, Downs JC. IOP-induced lamina cribrosa deformation and scleral canal expansion: Independent or related? Invest Ophthalmol Vis Sci. 2011b; 52 (12):9023–9032. [PubMed: 21989723]

Simo J, Taylor R, Pister K. Variational and projection methods for the volume constraint in finite deformation elasto-plasticity. Comput Meth appl Mech Eng. 1985; 51:177–208.

Storn R, Price K. Differential evolution–a simple and efficient heuristic for global optimization over continuous spaces. Journal of Global Optimization. 1997; 11 (4):341–359.

Taber LA, Humphrey JD. Stress-modulated growth, residual stress, and vascular heterogeneity. J Biom Eng. 2001; 123:528–535.

Watson PG, Young RD. Scleral structure, organisation and disease. a review. Exp Eye Res. Mar; 2004 78 (3):609–623. [PubMed: 15106941]

Watton PN, Ventikos Y, Holzapfe GA. Modelling the growth and stabilization of cerebral aneurysms. Math Med Biol. Jun; 2009 26 (2):133–164. [PubMed: 19234094]

Winkler M, Jester B, Nien-Shy C, Massei S, Minckler DS, Jester JV, Brown DJ. High resolution three dimensional reconstruction of the collagenous matrix of the human optic nerve head. Brain Res Bul. 2010; 81 (3):339–348.

Woo SL, Kobayashi AS, Schlegel WA, Lawrence C. Nonlinear material properties of intact cornea and sclera. Exp Eye Res. 1972; 14:29–39. [PubMed: 5039845]

Zeinali-Davarani S, Raguin LG, Vorp DA, Baek S. Identification of in vivo material and geometric parameters of a human aorta: toward patient-specific modeling of abdominal aortic aneurysm. Biomech Model Mechanobiol. Oct; 2011a 10 (5):689–699. [PubMed: 21053043]

Zeinali-Davarani S, Sheidaei A, Baek S. A finite element model of stress-mediated vascular adaptation: application to abdominal aortic aneurysms. Comput Meth Biomech Biomed Eng. Apr. 2011b 14:803–817.

Appendix A. Microstructure based constitutive model

Let the function describing the strain energy density W of the scleral tissue be composed of three parts: the energy density related to the isotropic tissue response W_{iso}, the anisotropic collagen network W_{col}, and a pure hydrostatic part U

$$W = W_{\text{iso}} + W_{\text{col}} + U \quad \text{(A.1)}$$

The energy contribution of the ground substance is modeled using an isochoric *Neo-Hookean* material model (Simo et al., 1985)

$$W_{\text{iso}} = \frac{1}{2}\mu\left(J^{-2/3}\,\text{tr}\mathbf{C} - 3\right) \quad \text{(A.2)}$$

with $J = \det\mathbf{F}$ and $\mathbf{C} = \mathbf{F}^{\text{T}}\mathbf{F}$, where $\mathbf{F}$ is the deformation gradient. The model contains one material parameter, the shear modulus μ, which represents the isotopic stiffness of the tissue. The pure hydrostaic part U controls the compressibility of the of the material and is defined as

$$U = \frac{1}{2}\kappa(\ln J)^2 \quad \text{(A.3)}$$

where κ is the bulk modulus. The bulk modulus was set to $\kappa = 1000\mu$ to model the near incompressibility of the sclera.

Let θ^i be a curvilinear spherical coordinate system that was fit to the posterior scleral shell with the polar axis going through the center of the lamina cribrosa (see Figure 1). The

related (orthonormal) base vectors $\mathbf{G}_i = \partial\mathbf{X}/\partial\theta^i$ can be obtained by standard derivations (Başar and Weichert, 2000) at any point $\mathbf{X}$. To define the collagen fibril architecture, the orthonormal basis $\mathbf{A}_i$ is introduced here. $\mathbf{A}_2$ is obtained from projection of the circumferential direction $\mathbf{G}_2$ onto the scleral surface, $\mathbf{A}_3$ is the normal vector of the experimentally obtained scleral surface and $\mathbf{A}_1 = \mathbf{A}_2 = \mathbf{A}_3$. Let $\mathbf{e}_0$ be a unit vector defined in the $\mathbf{A}_1$–$\mathbf{A}_2$ plane by means of an *Eulerian* angle $\phi \in [-\pi/2; \pi/2]$

$$\mathbf{e}_0(\varphi) = \sin(\varphi_p + \varphi)\mathbf{G}_1 + \cos(\varphi_p + \varphi)\mathbf{G}_2 \quad \text{(A.4)}$$

where ϕ_p is the angle that defines the preferred orientation of the collagen fibril network (see meso-scale in Figure 1). The axial stretch λ_{axial} of one collagen fibril pointing in direction ϕ can be computed as

$$\lambda_{\text{axial}}(\varphi) = (\mathbf{e}_0(\varphi)\mathbf{C}\mathbf{e}_0(\varphi))^{1/2} \quad \text{(A.5)}$$

This axial stretch can be used to compute the energy contribution of collagen fibrils $W_{\text{fib}}(\lambda_{\text{axial}}(\phi))$ pointing in the direction ϕ based on the microstructure-oriented model, which was developed by Grytz and Meschke (2009) for modeling crimped collagen fibrils. Please see the original paper for detail derivations of W_{fib}. The collagen network is assumed to be composed of collagen fibrils with distributed orientations $\mathbf{e}_0$. We use a normalized *von Mises* distribution function ρ to define the in-plane distributed collagen fibrils (Grytz, 2008; Girard et al., 2009b)

$$\rho(\varphi) = \frac{\exp(b\cos(2\varphi))}{I_0(b)\,\pi} \quad \text{(A.6)}$$

where b is the concentration parameter and I_0 the modified *Bessel* function of the first kind and order zero. The strain energy function of the collagen network is represented by the integral over the strain energy contributions of the collagen fibrils weighted by the distribution function ρ

$$W_{\text{col}} = \int_{-\pi/2}^{\pi/2} \rho(\varphi)\, W_{\text{fib}}(\lambda_{\text{axial}}(\varphi))\, d\varphi \quad \text{(A.7)}$$

We use a standard *Gauss-Legendre* quadrature of 15th order to numerically compute the above integral. For further derivation including the computation of stress and elasticity tensors please see our previous work (Grytz, 2008; Girard et al., 2009b).

To investigate the changing IOP-dependent elastic properties of the sclera at the different length scales of the purposed constitutive model, we introduce the *in-plane strain* ε_{IP}

$$\varepsilon_{\text{IP}} = J\left(\mathbf{A}_3\mathbf{C}^{-1}\mathbf{A}_3\right)^{1/2} - 1 \quad \text{(A.8)}$$

the collagen network strain ε_{col}

$$\varepsilon_{\text{col}}=\int_{-\pi/2}^{\pi/2}\rho(\varphi)\,(\lambda_{\text{axial}}(\varphi)-1)d\varphi \quad \text{(A.9)}$$

and collagen fibril strain ε_{fib}. The fibril strain is derived from the micro-scale model for crimped collagen fibrils. Please see Figure 1 for a graphical interpretation and the original paper for a detailed derivation of ε_{fib} (Grytz and Meschke, 2009). Furthermore, the percentile of locked collagen fibrils is introduced

$$\vartheta_{\text{lock}}=\frac{100}{\pi}\int_{-\pi/2}^{\pi/2}H(\lambda_{\text{axial}}(\varphi))d\varphi$$
$$\text{with } H(\lambda_{\text{axial}})=\begin{cases}0, & \lambda_{\text{axial}}<\lambda_{\text{lock}}\\ 1, & \lambda_{\text{axial}}\geq\lambda_{\text{lock}}\end{cases} \quad \text{(A.10)}$$

where λ_{lock} represents the locking stretch at which collagen fibrils straighten (uncrimp).

Appendix B. Cost function

We propose a following cost function as an objective function to estimate the quality of the inverse parameter fitting.

$$cost=\sum_{p=1}^{9}\frac{\int_\Omega(\mathbf{u}_p^{\text{FE}}-\mathbf{u}_p^{\text{exp}})\mathbf{W}_p(\mathbf{u}_p^{\text{FE}}-\mathbf{u}_p^{\text{exp}})dA}{\int_\Omega\mathbf{u}_p^{\text{exp}}\mathbf{W}_p\mathbf{u}_p^{\text{exp}}dA} \quad \text{(B.1)}$$

Herein, $\int_\Omega \mathrm{d}A$ represents the integration over the outer surface of the posterior scleral shell. The numerator in the above term represents the weighted integral of squared residuals between the finite element displacements $\mathbf{u}^{\text{FE}}$ and the experimental displacements $\mathbf{u}^{\text{exp}}$ integrated over the outer surface of the sclera. We use the denominator to normalize the residuals with the squares of experimental displacements such that the cost related to each IOP p has a similar impact on the total cost, where p represents the nine IOP elevations from 5 mmHg to: 7, 10, 15, 20, 25, 30, 35, 40, 45 mmHg. In equation (B.1), $\mathbf{W}_p$ is a weighting tensor which is used to account for large differences in the three displacement components with respect to the spherical coordinate system.

$$\mathbf{W}_p=\begin{bmatrix}w_{11}&0&0\\0&w_{22}&0\\0&0&w_{33}\end{bmatrix}_p\mathbf{G}^i\otimes\mathbf{G}^j \quad \text{(B.2)}$$

The components of the weighting tensor are defined in the following.

$$(w_{ii})_p=1-\frac{\int_\Omega|\mathbf{u}_p^{\text{exp}}\cdot\mathbf{G}_i|dA}{\int_\Omega(|\mathbf{u}_p^{\text{exp}}\cdot\mathbf{G}_1|+|\mathbf{u}_p^{\text{exp}}\cdot\mathbf{G}_2|+|\mathbf{u}_p^{\text{exp}}\cdot\mathbf{G}_3|)dA} \quad \text{(B.3)}$$
$$\text{for } i=1,2,3$$

Herein, $\mathbf{G}_i$ are the base vectors of the spherical coordinate system introduced in Appendix Appendix A. To penalize unphysical solution based on the tissue volume containing straighten scleral collagen fibrils the following dynamic penalty term was used.

$$penalty = (0.5 \cdot iter)^2 \left[\vartheta_{\mathrm{lock,tot}}(45) - \vartheta_{\mathrm{lock,tot}}(5) - 80\right]^2 \quad \text{(B.4)}$$

$\vartheta_{\mathrm{lock,tot}}(p)$ represents percentile of locked collagen fibrils of the entire posterior scleral shell at the IOP level p (mmHg) and *iter* is the current iteration of the DE algorithm. The pressure on unphysical solutions is increasing with increasing iteration steps due to the first term in (B.4). The penalty term (B.4) was added to the cost function (B.1) if less than 80% of scleral collagen fibrils were straighten for an IOP elevation from 5 to 45 mmHg. The objective function f used to evaluate the DE population was defined as

$$f = \begin{cases} cost + penalty & \text{if } \vartheta_{\mathrm{lock,tot}}(45) - \vartheta_{\mathrm{lock,tot}}(5) < 80 \\ cost & \text{otherwise} \end{cases}$$

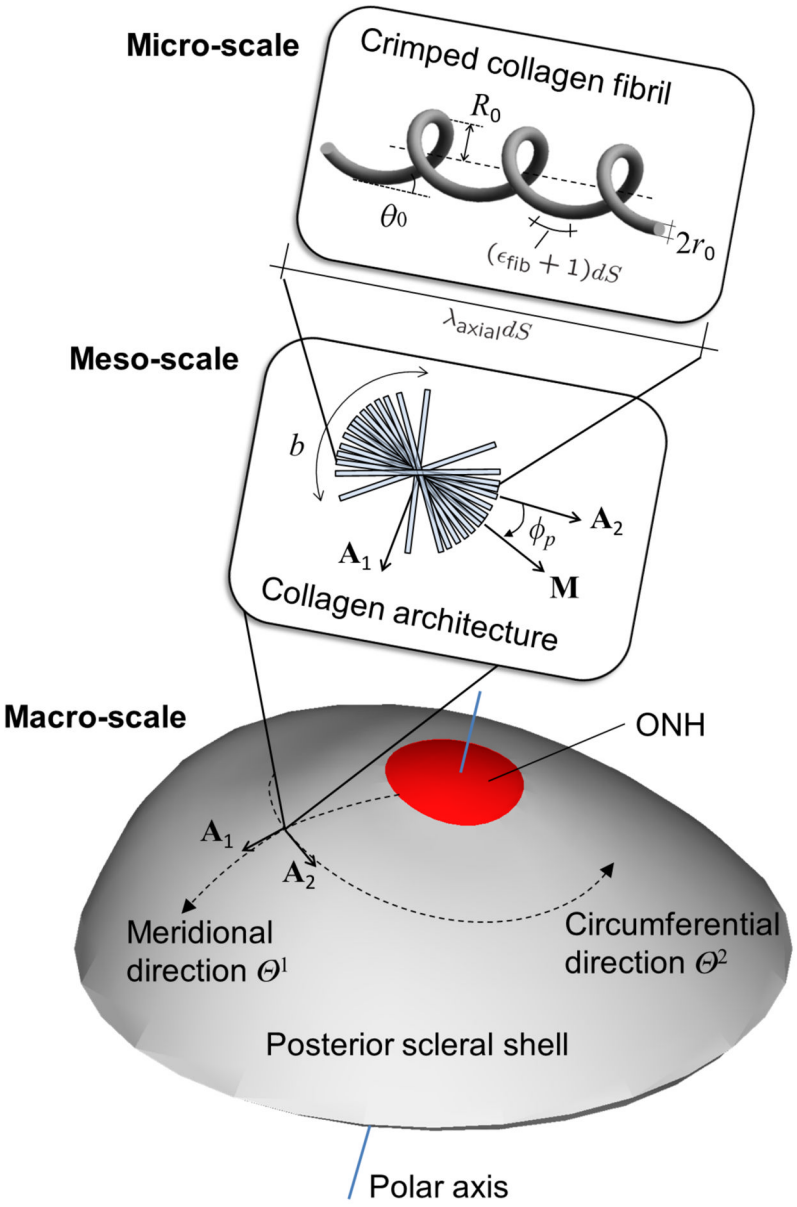

Figure 1.

Multi-scale model of the posterior scleral shell. At the macro-scale, a spherical coordinate system θ^i is defined that fits the scleral surface best with the polar axis going through the center of the ONH. $\mathbf{A}_1$ and $\mathbf{A}_2$ are base vectors projected onto the scleral surface following the meridional θ^1 and circumferential direction θ^2. At the meso-scale, the collagen architecture is represented by one family of collagen fibrils assuming a *von Mises* distribution of the fibril orientations. ϕ_p – the angle that defines the preferred orientation **M** with respect to the circumferential direction $\mathbf{A}_2$; b – the concentration parameter that defines the degree of alignment of the collagen fibrils with respect to the preferred orientation **M** ($b = 0$: randomly distributed fibrils in the scleral plane; $b = \infty$: perfectly aligned fibrils along **M**). At the micro-scale, collagen fibrils are assumed to crimp into a helix when the sclera is unloaded. λ_{axial} illustrates the stretch in the axis of a collagen fibril, which is used to calculate the average collagen network strain, and ε_{fib} illustrates the collagen fibril strain at

the micro-scale. θ_0 – the crimp angle; R_0 – the radius of the helix; r_0 – the radius of the collagen fibril crossection.

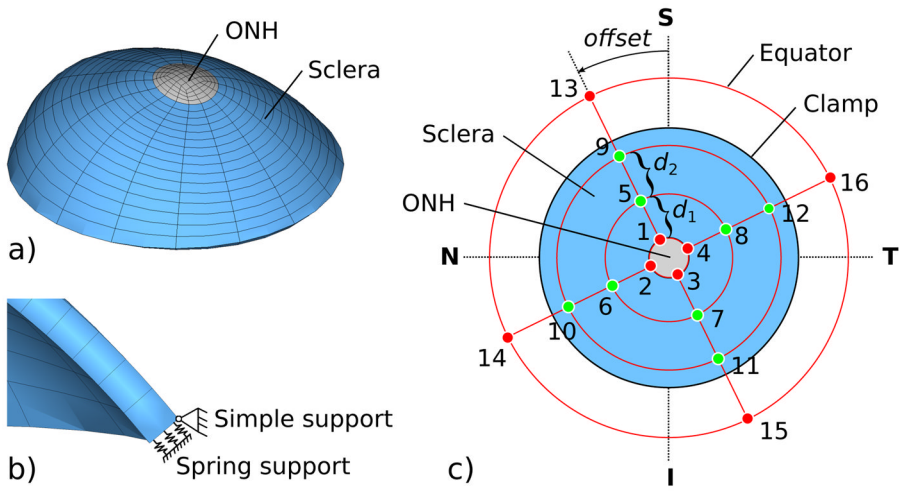

Figure 2.

(a) The eye-specific FE mesh of one eye showing the posterior scleral shell and the lamina cribrosa. The mesh captures the original shape and thickness of each eye. (b) Section through the FE mesh showing the boundary conditions at the clamp, including the simple support at the outer surface and the spring support through the scleral thickness. (c) The extended mesh (red lines) used to model local variations in the collagen fibril architecture by interpolating the meso-structural parameters (ϕ_p, b) between the control points (red and green circles). A standard bi-linear interpolation of the control point values is performed in the spherical coordinate space for each element of the extended mesh. The extended mesh extends beyond the posterior scleral boundaries, where control points 13–16 are located at the virtual equator of the eye. d_1, d_2 represent variable meridional distances. The extended mesh can be rotated by an offset angle offset. The meso-structural parameters (ϕ_p, b) are pre-defined at the red control points and fitted at the green control points.

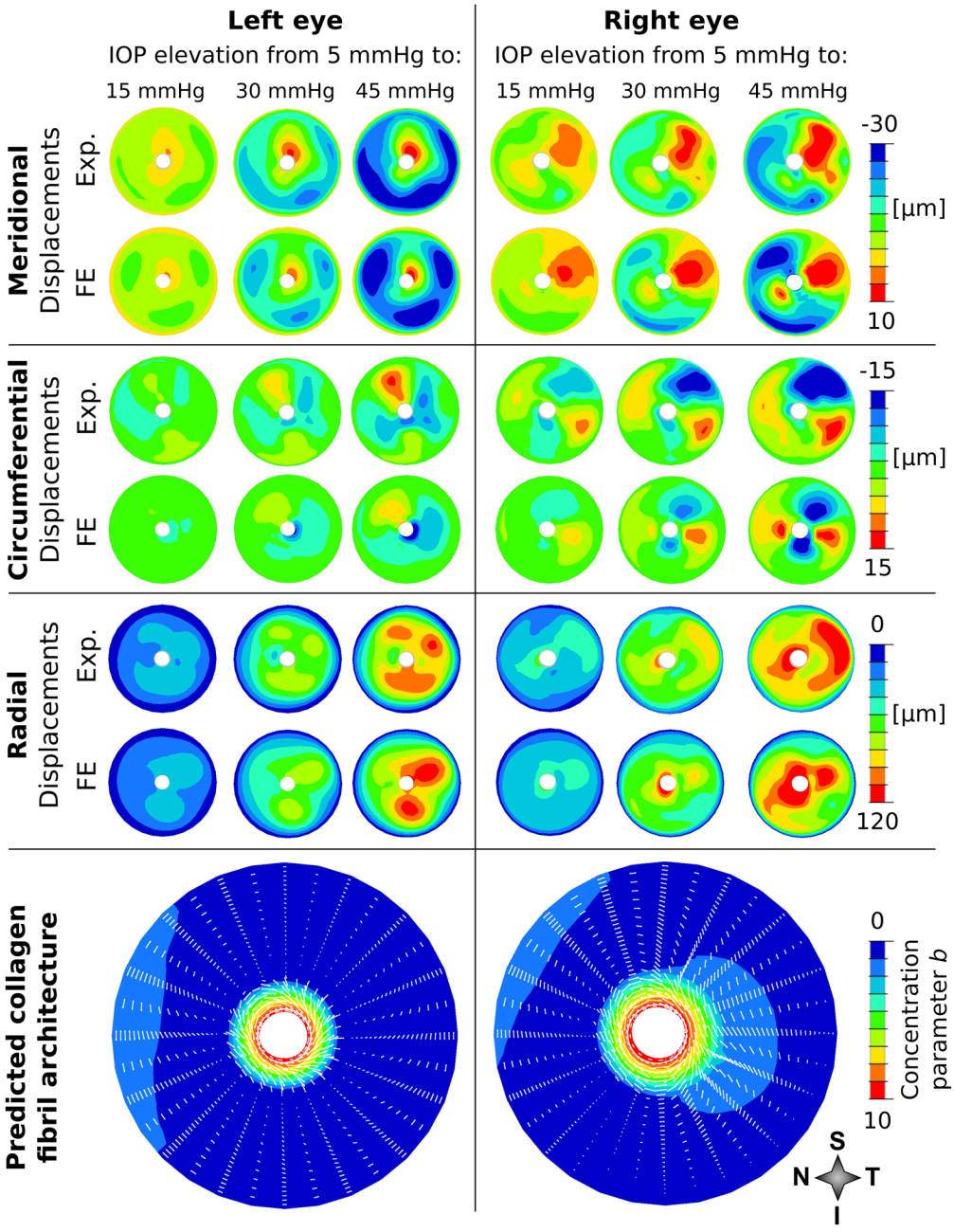

Figure 3.

Top: columns show the comparison of experimentally-measured and FE model-predicted displacements for both eyes (both shown in right eye configuration) of one donor (81 years old) for three IOP elevations from 5 to 15, 30, and 45 mmHg. The rows show the comparison between the experimentally measured and computationally predicted meridional, circumferential, and radial surface displacements. Column and row-wise comparisons show that the predicted displacements are in good agreement with both: (i) the overall nonlinear displacement response and (ii) the localized deformation patterns of the experimental measurements. Bottom: the predicted collagen fibril architecture for both eyes showing the concentration of collagen fibrils (contour plot) along their preferred orientations

(white lines). A ring of circumferentially aligned collagen fibrils is seen in the peripapillary scleral region around the scleral canal. Exp, Experimental.

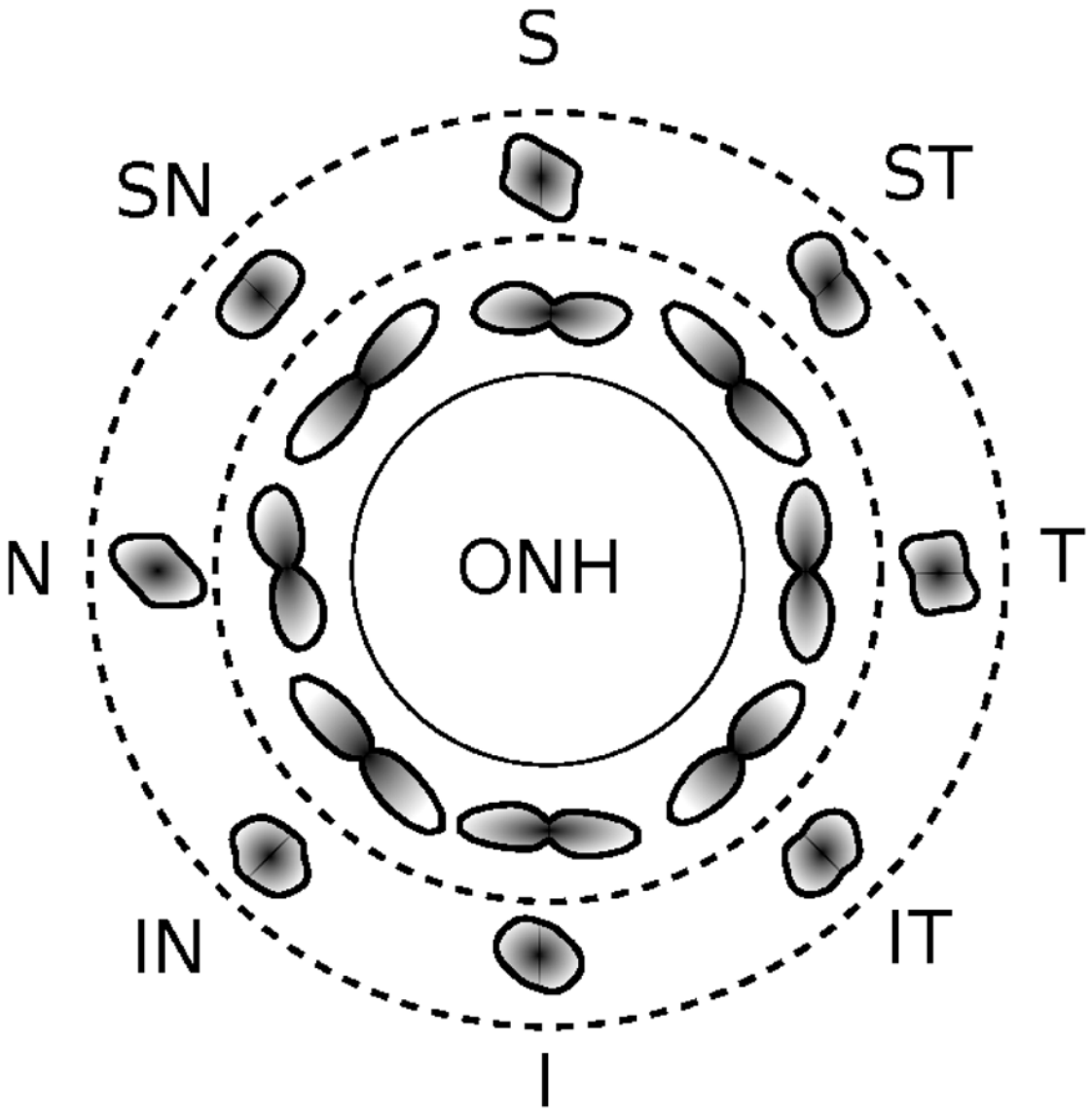

Figure 4.

Average collagen fibril density distributions in 8 sectors of the peripapillary and mid-peripheral region of the sclera averaged over all eyes, as represented by individual polar plots of the average collagen fibril distribution at each sector location. A high concentration of collagen fibrils in the circumferential direction can be seen across all sectors of the peripapillary region. More randomly organized collagen fibril orientations are observed in the mid-peripheral region.

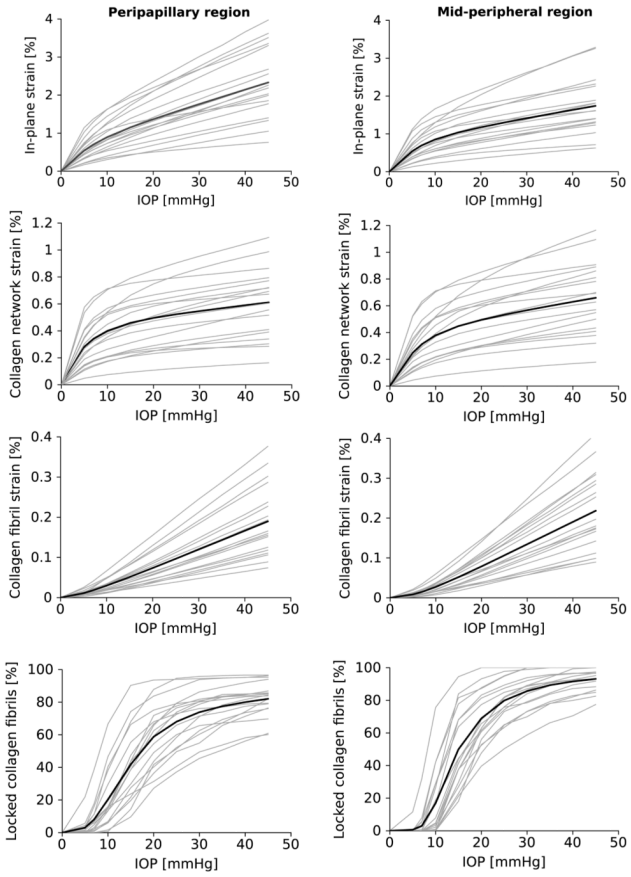

Figure 5.

From top to bottom, IOP versus the average in-plane strain, average collagen network strain, the average collagen fibril strain, and the percentile of locked collagen fibrils plots showing the model responses of all scleral shells (grey lines) and the mean response (black lines) for the peripapillary scleral (left plots) and mid-peripheral region (right plots). The in-plane strain and collagen network strain curves show the nonlinear and IOP-dependent stiffening of the sclera, while the collagen fibril strain increases nearly linear with increasing IOP. The average in-plane strain is higher in the peripapillary region than in the mid-periphery, while the average collagen network and fibril strains are almost identical for both regions. Collagen fibrils start to lock at about 7 mmHg and more fibrils get recruited to bear the load for increasing IOP. All plots show a significant variability in the data set.

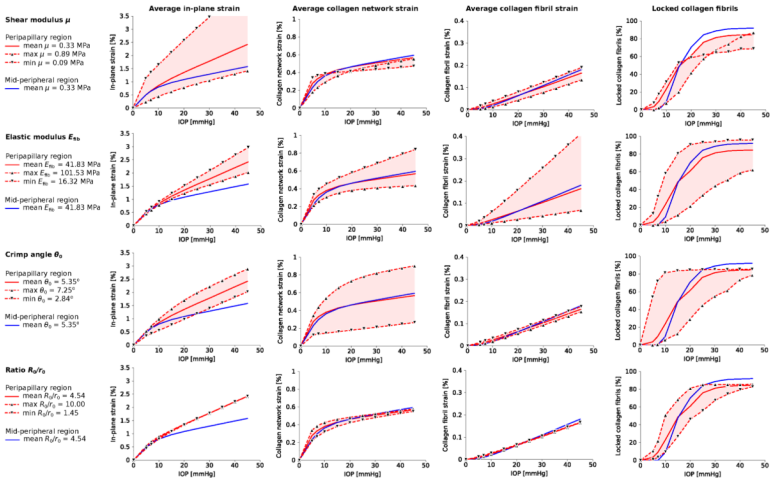

Figure 6.

Parameter study using the posterior scleral shell from the right eye of Donor 7 and the range of model parameters obtained from the fitting analysis using the full range of fitted parameters found in all the eyes. The influence of the two stiffness parameters (shear modulus of the tissue, elastic modulus of collagen fibrils) and two micro-structural parameters (collagen fibril crimp angle and ratio R_0/r_0) on the IOP-dependent responses is shown for the peripapillary scleral (red) and mid-peripheral region (blue): from left to right, the average in-plane strain, average collagen network strain, the average collagen fibril strain, and the percentile of locked collagen fibrils. For each parameter, the response for the maximum (dashed line with triangles up), minimum (dashed line with triangles down) and mean values (solid lines) are compared, while keeping the other model parameters at their mean values. The fitted meso-structural parameters (b, ϕ_D) were not varied.

Table 1

Fitted parameters describing the scleral material response, including the assumed lower and upper limits of the parameter search space. The limit values in brackets represent the bounds of the first random population of the global differential evolution method (Section 2.4.2) if different from the parameter search space.

Parameter		Number of unknowns	Lower limits	Upper limits
Micro-scale (collagen fibril):				
θ_0	crimp angle	1	2°	∞ (8°)
R_0/r_0	ratio between crimp amplitude and cross-section radius	1	1	10
E_{fib}	elastic modulus of the collagen fibrils	1	10.0 MPa	∞ (100 MPa)
Meso-scale (collagen architecture):				
$\phi_{p,5}$–$\phi_{p,8}$	preferred collagen fibril orientations at each control point 5–8	4	−90°	90°
$\phi_{p,9–12}$	one preferred collagen fibril orientation for control points 9–12	1	−90°	90°
b_5–b_{12}	collagen fibril concentration parameters at each control point 5–12	8	0	∞ (5)
Macro-scale (posterior scleral shell):				
μ	shear modulus of the tissue	1	0.01 MPa	∞ (1 MPa)
k	surface spring stiffness for the clamping boundary condition	1	0	∞ (100 N/mm^3)
offset	circumferential offset of the extended mesh	1	−45°	45°
d_1	meridional distance between control points 1–4 and 5–8	1	5°	15°
d_2	meridional distance between control points 5–8 and 9–12	1	15°	45°
Total		21		

Table 2

The fitted material and microstructural parameters, as well as the optimized cost, calculated for five independent trials of the inverse fitting process for both eyes of Donor 1.

Eye	Trial	Shear modulus μ [MPa]	Elastic modulus E_{fib} [MPa]	Crimp angle θ_0 [deg]	Ratio R_0/r_0	Cost
	1	0.0643	27.4791	6.4732	4.6019	1.0313
	2	0.0643	27.4774	6.4734	4.5996	1.0313
Right	3	0.0644	27.4974	6.4719	4.6180	1.0313
	4	0.0644	27.5238	6.4727	4.6194	1.0313
	5	0.0643	27.4605	6.4735	4.6016	1.0313
Max. diff.		0.25%	0.23%	0.03%	0.43%	0.00%
	1	0.5867	22.5453	3.7879	1.9108	0.4596
	2	0.5863	22.5503	3.7881	1.9090	0.4596
Left	3	0.5867	22.5296	3.7878	1.9117	0.4596
	4	0.5866	22.5337	3.7872	1.9093	0.4596
	5	0.5864	22.5524	3.7878	1.9102	0.4596
Max. diff.		0.08 %	0.10 %	0.02 %	0.14 %	0.00 %

Table 3

The fitted stiffness and microstructural parameters including the optimized cost of the inverse models of the 18 donor eyes. M, male; F, female; R, right; L, left; STDEV, standard deviation.

Donor	Sex	Age	Eye	Shear modulus μ [MPa]	Elastic modulus E_{fib} [MPa]	Crimp angle θ_0 [deg]	Ratio R_0/r_0	Cost
1	M	81	R	0.13	27.48	6.47	4.60	1.03
			L	0.59	22.53	3.79	1.91	0.46
2	M	80	R	0.45	45.48	4.49	3.29	0.41
			L	0.29	24.79	6.08	2.51	0.69
3	F	66	R	0.25	42.30	6.31	4.19	0.72
			L	0.11	32.67	6.99	10.00	1.41
4	F	77	R	0.82	71.51	3.87	5.03	0.84
			L	0.09	23.83	6.92	4.00	0.61
5	F	82	R	0.18	25.48	6.10	5.59	1.29
			L	0.26	25.49	5.16	3.50	1.23
6	M	90	R	0.24	59.83	4.49	2.04	0.32
			L	0.42	35.50	5.26	4.40	0.83
7	M	78	R	0.37	40.69	5.58	4.73	0.81
			L	0.21	19.31	7.25	2.37	0.68
8	M	88	R	0.40	16.32	3.97	10.00	0.84
			L	0.69	67.23	2.84	1.45	0.66
9	F	57	R	0.23	70.97	6.21	8.98	0.92
			L	0.26	101.53	4.54	3.10	1.31
Mean		77.67		0.33	41.83	5.35	4.54	0.84
STDEV		10.05		0.20	23.37	1.28	2.63	0.31

J Mech Behav Biomed Mater. Author manuscript; available in PMC 2015 January 01.